# 4 Electronic Structure of Condensed Matter

## 4-1 Direct Observation of One-dimensional Electronic States in Single-wall Carbon Nanotubes

In one-dimensional (1D) metals, the Fermi-liquid states applicable to 3D conventional metals become unstable to Coulomb interaction and the conduction electrons behave as a Tomonaga-Luttinger-liquid (TLL). This TLL state is characterized by interaction-dependent anomalous exponents seen in the correlation functions. Metallic single-wall carbon nanotubes (SWNTs) are considered to be ideal 1D systems for realizing TLL states [1]. It is interesting to investigate directly the electronic states of SWNTs. The photoemission experiments were performed at BL-11D of KEK-PF and BL-1 of HiSOR [2]. SWNT samples were prepared by the laser vaporization method. The mean diameter of SWNTs in the sample is 1.37 nm.

A SWNT is made of a 2D graphite sheet rolled into a cylindrical shape [3]. The electronic states along the circumference are quantized so that peak structures due to 1D van Hove singularities (1D VHS) appear in the density of states. Fig. 1 shows the photoemission spectra of SWNT sample and graphite measured at $h\nu$=65 eV. The valence band spectrum of the SWNT is similar as a whole to that of graphite. The difference in spectral features between the SWNT and graphite appeared in the energy region near the Fermi level ($E_F$). For the SWNT sample, three peak structures denoted by $S_1$, $S_2$ and $M_1$ can be clearly seen around the binding energies of 0.45, 0.75 and 1.0 eV, respectively. The structure and electronic properties of SWNTs can be defined by the so-called chiral index expressed in ($n_1$, $n_2$) [3]. For SWNTs with diameters near 1.37 nm, for example, a metallic SWNT with a chiral index (10, 10) has a diameter of 1.375 nm and a semiconducting SWNT with (16, 2) has a diameter of 1.357 nm. The densities of states for the SWNTs with these chiral indices are also shown in Fig. 1. As can be seen from the figure, the $S_1$ and $S_2$ peaks and the $M_1$ peak can correspond to the 1D VHS structures coming from semiconducting and metallic SWNTs, respectively.

Fig. 2 shows the high-resolution photoemission spectra near $E_F$. The observed photoemission intensity decreases rapidly near $E_F$. This spectral feature is different from that of Au (3D conventional metal). As the origin of the peculiar spectral feature near $E_F$, we consider the suppression in density of states near $E_F$ seen in a TLL state. The theoretical calculation for the TLL state in the metallic SWNT was performed; the calculated spectrum has a spectral function of $\omega^{0.4}$ at zero temperature, where $\omega$ is the energy measured from $E_F$; the intensities at $E_F$ show a power-law dependence on temperature ($T^{0.4}$) [4]. The observed spectral features are not contradictory to the theoretical calculation of the TLL state. From fitting with $\omega^{\alpha}$, the exponent $\alpha$ was estimated to be 0.46 ± 0.10. In Fig. 2 inset, we plotted the intensities at $E_F$ as a

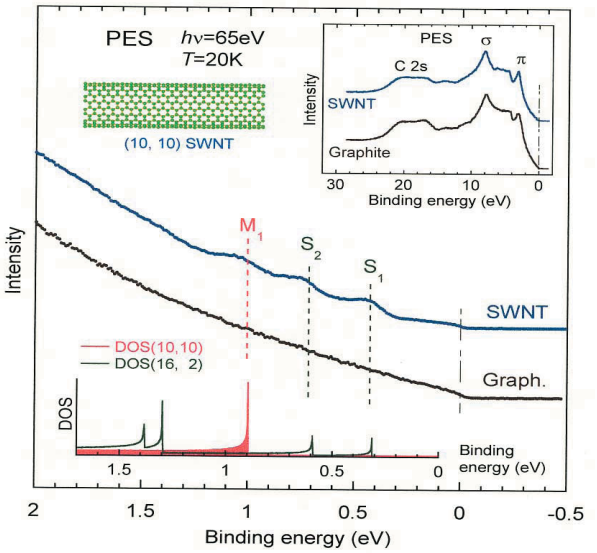


Figure 1
Photoemission spectra (PES) of SWNT sample and graphite. The densities of states (DOS) for SWNTs with chiral indices (10, 10) and (16, 2) are also shown. The spectrum of the SWNT sample was shifted toward a higher binding energy by 0.1 eV because of doping of the SWNTs by Cu substrate.

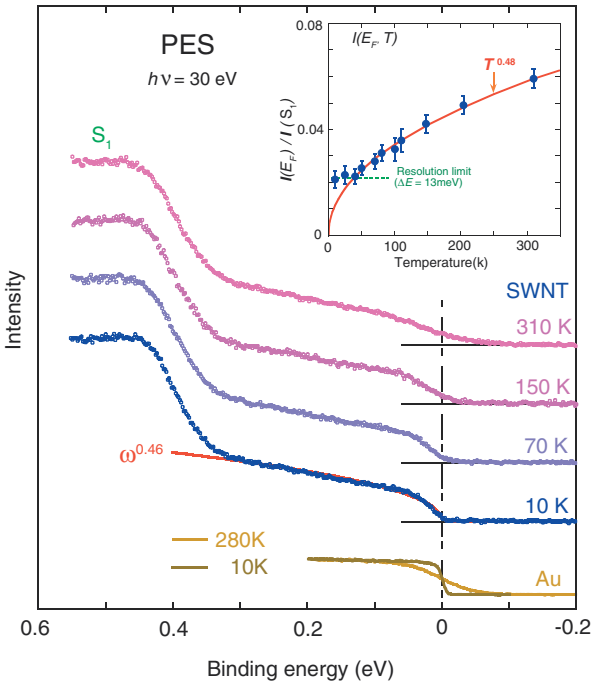


Figure 2
Photoemission spectra (PES) of SWNT sample near $E_F$. A solid line indicates $\omega^{0.46}$ broadened by the energy resolution ($\Delta E$ = 13 meV). The inset shows the temperature dependence of the ratio of the intensity at $E_F$ to the intensity of the $S_1$ peak.

function of temperature. The intensities are proportional to $T^{0.48\pm0.08}$. An important point is that almost the same exponent $\alpha$ as the spectral function was obtained. These power-law behaviors show good agreement with the theoretical calculation [1,4] and consistent with the results obtained from previous transport experiments [5]. We have found direct evidence that a TLL state is realized in SWNTs.

**H. Ishii[1], H. Kataura[1], H. Shiozawa[1], H. Yoshioka[2], H. Otsubo[1], Y. Takayama[1], T. Miyahara[1], S. Suzuki[1], Y. Achiba[1], M. Nakatake[3], T. Narimura[4], M. Higashiguchi[4], K. Shimada[5], H. Namatame[5] and M. Taniguchi[4, 5]**
**([1]Tokyo Metro. Univ., [2]Nara Women's Univ., [3]KEK-PF, [4]Hiroshima Univ., [5]HiSOR)**

## References

[1] R. Egger and A. O. Gogolin, *Phys. Rev. Lett.*, **79**, 5082 (1997).
[2] H. Ishii, H. Kataura, H. Shiozawa, H. Yoshioka, H. Otsubo, Y. Takayama, T. Miyahara, S. Suzuki, Y. Achiba, M. Nakatake, T. Narimura, M. Higashiguchi, K. Shimada, H. Namatame and M. Taniguchi, *Nature,* **426**, 540 (2003).
[3] R. Saito, G. Dresselhaus and M. S. Dresselhaus, *Physical Properties of Carbon Nanotubes* (Imperial College Press, London, 1998).
[4] H. Yoshioka, *Physica E,* **18**, 212 (2003).
[5] M. Bockrath, D. H. Cobden, J. Lu, A. G. Rinzler, R. E. Smalley, L. Balents and P. L. Mceuen, *Nature,* **397**, 598 (1999).

# 4-2 Fermi Surface of a Shape Memory Alloy of TiNi

Equiatomic TiNi is the most technologically important shape memory alloy. Upon cooling, it undergoes a martensitic transformation from a high-temperature CsCl-type phase, called the B2 or β-phase, to a monoclinic phase. The crystallographic and metallurgical aspects of martensitic transformations have been extensively studied so far. Current interest has been on the precursor where anomalies in the elastic constants and phonon spectra are commonly observed in all martensitic alloys. Inelastic neutron scattering experiments on TiNi have found that the $TA_2$[110] phonon branch in the β-phase becomes soft near $Q_0 = 1/3[110]2\pi/a$ at approximately room temperature[1], where a is the lattice constant. The origin of the phonon softening has long been speculated to be due to Fermi surface nesting. Several theoretical calculations of the band structure and the Fermi surface of TiNi have been performed. So far, however, no direct experimental information about the geometry of the Fermi surface of the β-phase has been obtained simply because no traditional spectroscopy for Fermiology could be applied to the high-temperature phase. Recently, it has become possible to map out the three-dimensional (3D) Fermi

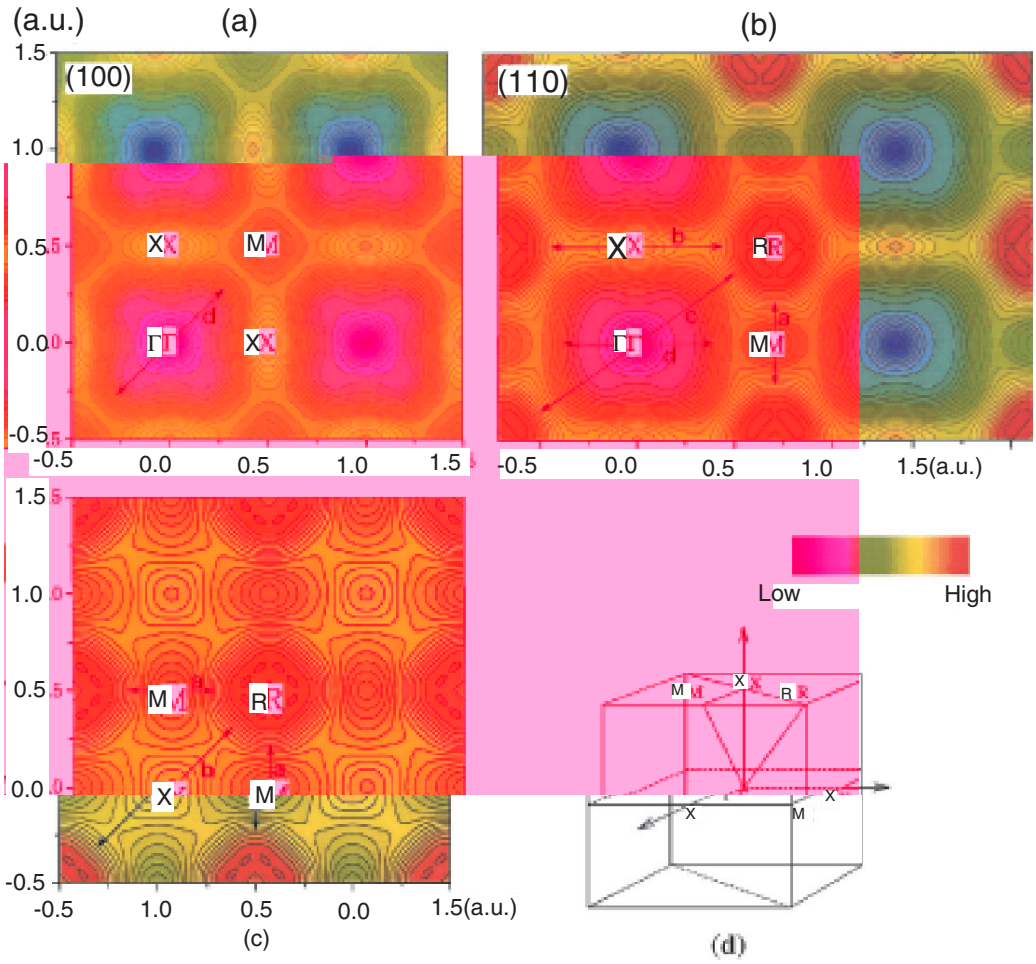


Figure 3
Contour maps of the occupation number densities on the Γ-X-M (a), Γ-X-R-M (b) and X-M-R (c) planes in the repeated zone scheme. The first Brillouin zone with high symmetry points is depicted in (d). The arrows indicate possible nesting vectors. Reproduced from Ref. [3].

surface of metals, alloys and compounds in almost any environment by reconstructing the 3D electron momentum density from Compton scattering data [2].

Here, we present the occupation number density in *k*-space (the first Brillouin zone) of $Ti_{48.5}Ni_{51.5}$ obtained from Compton scattering data, and examine the geometry and nesting feature of the Fermi surface [3].

An alloy ingot of $Ni_{51}Ti_{49}$ was prepared from pure nickel (99.97 %) and sponge titanium (99.875 %) by repeated arcmelting in a high-purity argon atmosphere. A single crystal was grown from the ingot by a floating zone melting method. The martensitic transformation temperature Ms ($A_f$) of the specimen was found to be 170 K (210 K). The Compton profiles were measured at AR-NE1A1. Directional Compton profiles along 28 independent directions were measured. The overall instrumental resolution was 0.13 atomic units (a.u.) in full width at half maximum. The direct Fourier transform method [2] was applied to reconstruct the 3D electron momentum density $\rho(p)$. After obtaining $\rho(p)$, we employed the LCW-folding procedure [4] to obtain the 3D occupation number density in *k*-space.

Figs. 3(a)-3(c) show the contour maps of the occupation number densities on the Γ-X-M, Γ-X-R-M and X-M-R planes, respectively, in the repeated zone scheme. The planes and symmetry points of the first Brillouin zone are shown in Fig. 3(d). The occupation number density is the lowest at Γ and the highest at R and X, indicating the presence of a hole surface centered at Γ and electron surfaces at R and X. We can easily recognize the geometrical shape of the Fermi surface. With regard to the nesting features of the Fermi surface, exercising purely geometrical consideration on the pattern of contours, we see some parallel or near parallel flat surfaces which suggest possible nesting. For intraband nesting of the parallel flat parts of the electron surface at R there are two nesting vectors, *a* in parallel with the R-M-R axis and *b* in parallel with the R-X-R axis as shown by the arrows in Fig. 3(c), and a vector *c* in parallel with the R-Γ-R axis in Fig. 3(b). The length of the arrows does not indicate the exact length of the nesting vectors because the exact edge of the Fermi surface is blurred due to the experimental resolution. For another intraband nesting of the near parallel flat parts of the hole surface centered at Γ, there is a vector *d* in parallel with the Γ-M axis as shown in Fig. 3(a). Let us focus on the nesting vector *b* in the [110] direction, whose length is approximately 2/3[110]2π/a. By recalling the expression of the generalized susceptibility, it can be reduced to 1/3(110)2π/a by subtracting the [110] reciprocal lattice vector. Thus, we have succeeded, for the first time from an experimental point of view, to show that the phonon softening mentioned above originates from this nesting vector *b*.

**N. Shiotani[1], I. Matsumoto[1], H. Kawata[1], J. Katsuyama[2], M. Mizuno[2], H. Araki[2] and Y. Shirai[2]**
**([1]KEK-PF, [2]Osaka Univ.)**

## References

[1] H. Tietze, M. Müllner and B. Renke, *J. Phys. C: Solid State Phys.,* **17** (1984) L529.
[2]Y. Tanaka, Y. Sakurai, A. T. Stewart, N. Shiotani, P. E. Mijnarends, S. Kaprzyk and A. Bansil, *Phys. Rev. B,* **63** (2001) 045120.
[3] N. Shiotani, I. Matsumoto, H. Kawata, J. Katsuyama, M. Mizuno, H. Araki and Y. Shirai, *J. Phys. Soc. Jpn.*, **73** (2004) 1627.
[4] D. G. Lock, V. H. C. Crisp and R. N. West, *J. Phys. F: Met. Phys.,* **3** (1973) 561.

# 4-3 Magnetic Circular Dichroism of Resonant X-ray Emission Spectroscopy in Sm-Co Amorphous Alloy

Electric quadrupolar (E2) transitions at the rare-earth (R) $L_{3,2}$-edges have attracted wide interest as an important subject for solid-state spectroscopy and for X-ray studies of magnetism, since the 4f final state of the $2p \rightarrow 4f$ quadrupolar transition is the dominant magnetic carrier of R elements. It has been widely believed that the E2 contribution has an absorption signal at the pre-edge regions of the $L_{2,3}$-edges, since the $4f$ level is pulled down below the dipolar (E1) absorption edge due to the strong Coulomb interaction between the $2p$ core hole and the $4f$ electrons. Although the E2 contributions are not normally visible in X-ray absorption spectroscopy (XAS) spectra due to their being superimposed on the E1 transition, they are significantly enhanced in magnetic circular dichroism (MCD) spectra as shown in Fig. 4. However, confirmation of this has been a controversial subject for a long time due to the difficulty in collecting satisfactory evidence within the framework of first order optical processes such as MCD of XAS (MCDXAS).

In the present study, the E2 transition has been studied by means of resonant X-ray emission spectroscopy (RXES), a coherent second order optical process. It is a great advantage of RXES that the E2 contribution can be separated from the E1 transition judging from the energy scheme since the optical process is identified by the emission energy. RXES experiments at the Sm $L_{2,3}$-edges in $Sm_{21}Co_{79}$ amorphous film were performed at BL-28B using the "Escargot" X-ray emission spectrometer. Fig. 5 shows MCD spectra of RXES (MCDRXES) recorded for the $L_3M_{4,5}$ edges, which correspond to the optical process of the $3d \rightarrow 2p$ decay after the $2p \rightarrow 5d$ dipolar (E1) excitation and the $2p \rightarrow 4f$ quadrupolar (E2) excitation. In the MCDRXES spectrum at point (a) in Fig. 5, the E2 MCD features associated with $Q_1$ and $Q_2$ are observed with the negative and positive signs, respectively. The signs of peaks $Q_1$ and $Q_2$ for Fig. 5 are consistent with those of *a* and *b* in the MCDXAS in Fig. 4. For the MCDRXES spectrum of $Q_1$, the E2 contribution is confirmed to be the dominant origin of the corresponding MCDXAS because the E1 part has a dispersive shape, the integration of which is almost zero. The observation of the negative peak and the positive shoulder of MCDRXES for the $Q_1$

and $Q_2$ signals represents direct identification of the E2 MCD at the pre-edge region and is exactly what we have expected to obtain in the present experiment.

To interpret the experimental results, theoretical calculations based on the formula of the coherent second order optical process have been carried out. The calculated MCDRXES spectra reproduce all the experimental results very successfully (not shown here). The full experimental and theoretical results in the present study including the result for the Sm $L_2$-edge have been published as ref. [1]. A more recent theoretical work has also been published as ref. [2]. The series of the present study has given the important knowledge of how we use the E2 transition for the study of the 4f magnetism and how we interpret the result.

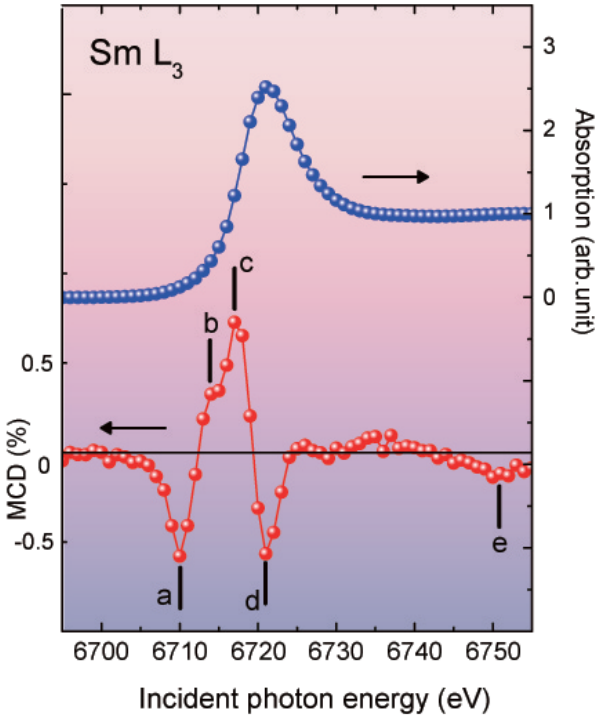


Figure 4
XAS (blue circle) and MCD (red circle) at the Sm $L_3$-edge in $Sm_{21}Co_{79}$ amorphous thin film at room temperature. Peaks *a* and *b* are attributed to originate from the E2 contribution at the pre-edge region. Energies *c*, *d* and *e* correspond to on- and off-resonant energy regions at the $L_3$-edge. The MCDRXES were recorded at the energies labeled by a ~ e.

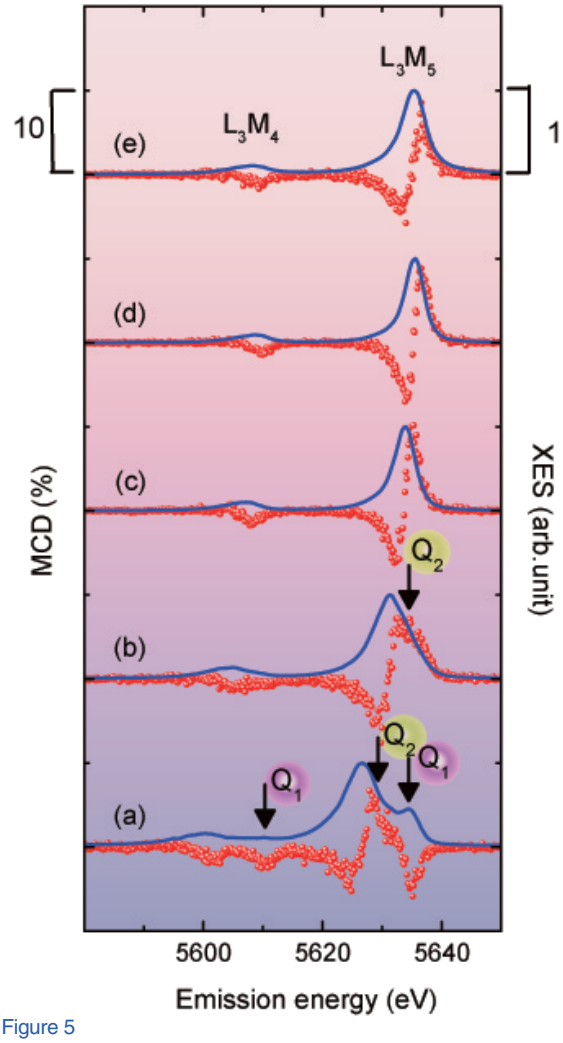


Figure 5
RXES (blue lines) and MCD spectra (red circles) for the Sm $L_3M_{4,5}$ edges. The labels a ~ e are consistent with those in Fig. 4. All the spectra have been normalized so that the peak intensity of RXES is 1. RXES peaks labeled $Q_1$ and $Q_2$ are due to the E2 transitions from $2p$ to $4f$, where $Q_1$ and $Q_2$ are attributed to be RXES which originate from the E2 excitation to the majority and the minority of the Sm $4f$ spin state, respectively.

**T. Nakamura[1], K. Fukui[2], T. Iwazumi[3], A. Kotani[2], H. Shoji[1], I. Harada[4], H. Ogasawara[2], E. Hirai[1], R. Katano[5], Y. Isozumi[5] and S. Nanao[1] ([1]IIS, Univ. of Tokyo, [2]ISSP, Univ. of Tokyo, [3]KEK-PF, [4]Okayama Univ., [5]RIRC, Kyoto Univ.)**

## References

[1] T. Nakamura, H. Shoji, E. Hirai, S. Nanao, K. Fukui, H. Ogasawara, A. Kotani, T. Iwazumi, I. Harada, R. Katano and Y. Isozumi, *Phys. Rev. B,* **67** (2003), 094439.
[2] K. Fukui and A. Kotani, *J. Phys. Soc. Jpn.*, **73** (2004), 1059.